

The impact of Rashba spin-orbit coupling in charge-ordered systems

Rodrigo A. Fontenele,¹ Sebastião dos Anjos Sousa Júnior,¹ Tarik P. Cysne,² and Natanael C. Costa¹

¹*Instituto de Física, Universidade Federal do Rio de Janeiro Cx.P. 68.528, 21941-972 Rio de Janeiro RJ, Brazil*

²*Instituto de Física, Universidade Federal Fluminense, 24210-346 Niterói RJ, Brazil*

We study the impact of the Rashba spin-orbit coupling (RSOC) on the stability of charge-density wave (CDW) in systems with large electron-phonon coupling (EPC). Here, the EPC is considered in the framework of the Holstein model at the half-filled square lattice. We start obtaining the phase diagram of the Rashba-Holstein model using the Hartree-Fock mean-field theory, and identifying the boundaries of the CDW and Rashba metal phases. As our main result, we notice that the RSOC disfavors the CDW phase, driving the system to a correlated Rashba metal. Proceeding, we employ a cluster perturbation theory (CPT) approach to investigate the phase diagram beyond the Hartree-Fock approximation. The quantum correlations captured by CPT indicate that the RSOC is even more detrimental to CDW than previously anticipated. That is, the Rashba metal region is observed to be expanded in comparison to the mean-field case. Additionally, we investigate pairing correlations, and the results further strengthen the identification of critical points.

I. INTRODUCTION

A growing class of two-dimensional (2D) materials offers opportunities to explore condensed-matter phenomena in a new and flexible platform¹⁻⁴. In addition to their technological applications, the prospect of solving some old puzzles in solid-state physics motivates much of the fundamental studies in this field. Graphene was the first genuinely 2D material synthesized, but apart from specific situations⁵, electronic correlations do not play a significant role on the observed properties, due to their highly dispersive band structure^{6,7}. Therefore, part of the research on 2D materials was developed within the single-particle perspective and neglecting many-body effects⁸. With the progress in the quality of samples and synthesis of novel families of materials, a renewed interest in the phases of matter driven by electronic correlation reappeared in the 2D materials community. Among those compounds of interest, we mention the superconducting phase in twisted bilayer graphene⁹, the magnetism in Cr₂Ge₂Te₆¹⁰ and CrI₃¹¹, and the charge-density wave (CDW) phase in some transition metal dichalcogenide (TMDs) family¹².

For a CDW phase, the key feature is the occurrence of an electron-phonon coupling (EPC), which creates instabilities in the metallic system, leading to a ground state with a spatially-modulated charge order^{13,14}. Such a state is characterized by a gapped single-particle charge spectrum and a gapless collective mode formed by phonon excitations. Interestingly, CDW and superconducting phases have been observed in TMDs compounds which stabilize in the centrosymmetric (1T)¹⁵ and the non-centrosymmetric (2H)¹⁶ structures. In addition, due to the high atomic number of transition metal atoms, the compounds in the TMD family typically have a strong *intrinsic* spin-orbit coupling (SOC). However, the interplay between the leading effects of a SOC and an EPC, regarding in particular how the SOC affects CDW formation, is still an open issue. Indeed, the study of the interplay between EPC and SOC in TMDs is challenging due to its

complex orbital nature and tri-layer structure, with some works suggesting a SOC-induced renormalization of the electron-phonon coupling^{17,18}.

Different types of spin-orbit interaction may also appear in materials depending on the point-group symmetries of their lattice structure. In addition to the intrinsic SOC characteristic of materials with high atomic numbers, other types of SOC can be induced in materials by *extrinsic* mechanisms. For instance, the Rashba SOC (RSOC) occurs in systems with broken ($z \rightarrow -z$)-symmetry, frequently appearing in surface-confined electrons of semiconductor heterostructures¹⁹, alloys^{20,21}, and surface-states of metallic systems²². It can also be induced in 2D materials by proximity to suitable substrates²³⁻²⁵. In this context, calculations using density functional theory indicate that pristine lead chalcogenides monolayers [PbX, with X = S, Se, Te] are 2D materials with strong RSOC²⁶. Its monolayers possess a buckled square lattice that breaks ($z \rightarrow -z$)-symmetry, allowing the occurrence of the Rashba effect, whose intensity is adjusted by changing the buckling angle, via application of strain²⁷. The RSOC may also occur in other 2D materials such as 2D perovskites, and Janus monolayer of transition metals dichalcogenides²⁸.

One significant impact of the RSOC is the emergence of a spin-dependent momentum shift, resulting in spin-splitting effects in the band structure. This spin splitting can have profound consequences on the electronic properties of the system, particularly on electron correlations, directly affecting the emergence of new phases. For instance, in certain families of iridates and pyrochlores – materials that demonstrate strong electron-electron and spin-orbit interactions – the interplay between RSOC and electron-electron interactions may give rise to topologically nontrivial states, Weyl semimetals, or even Kitaev spin liquids²⁹⁻³¹. Despite recent advancements in this field, the effects of RSOC on *electron-phonon* interacting systems, such as those compounds mentioned earlier, remain less clear.

In view of these stimulating results, in this paper we investigate the impact of RSOC in a charge-ordered sys-

tem. Here, we consider dispersionless phonon degrees of freedom coupled to the electrons, within the framework of the Holstein model³²: a simplified model whose ground state at the half-filled square lattice exhibits a staggered CDW phase for any electron-phonon coupling³³. This charge-ordered phase may undergo significant changes when external parameters are introduced – such as electronic doping^{34,35}, pressure or strain^{36,37}, nonlinear electron-phonon couplings^{38–40}, disorder⁴¹, doping with magnetic impurities⁴², or phonon dispersion⁴³ –, with the enhancement of pairing correlations for most of cases. Despite this scrutinization, the impact of a SOC on the Holstein CDW phase is barely unknown. We bridge this gap by examining the Rashba-Holstein Hamiltonian through two methodologies: mean-field (MF) and cluster perturbation theory (CPT) approaches.

The paper is organized as follows: we present the Rashba-Holstein model in Sec. II, with the results for the MF and CPT approaches being discussed in Secs. III and IV, respectively. In Section V we present our conclusions.

II. THE RASHBA-HOLSTEIN HAMILTONIAN

We consider electrons hopping in a single orbital square lattice. Here, we assume the system has a broken ($z \rightarrow -z$)–symmetry, as occurs in lead chalcogenides monolayers^{26,27} and in confined electron gases^{19–22}, which allows the occurrence of RSOC. In addition, we use the Holstein model to describe the electron-phonon coupling, which captures the local interaction of electrons with single-Einstein phonon degrees of freedom³².

For the Rashba-Holstein model, the Hamiltonian reads

$$\begin{aligned} \mathcal{H} = & -t \sum_{\langle \mathbf{i}, \mathbf{j} \rangle, \sigma} (c_{\mathbf{i}, \sigma}^\dagger c_{\mathbf{j}, \sigma} + h.c.) - \mu \sum_{\mathbf{i}, \sigma} n_{\mathbf{i}, \sigma} \\ & + \hbar \omega_0 \sum_{\mathbf{i}} a_{\mathbf{i}}^\dagger a_{\mathbf{i}} - g \sum_{\mathbf{i}, \sigma} n_{\mathbf{i}, \sigma} (a_{\mathbf{i}} + a_{\mathbf{i}}^\dagger) \\ & - t_R \sum_{\langle \mathbf{i}, \mathbf{j} \rangle} c_{\mathbf{i}}^\dagger (\overleftrightarrow{\alpha}_{\mathbf{i}, \mathbf{j}} \times \overleftrightarrow{\sigma})_z c_{\mathbf{j}}, \end{aligned} \quad (1)$$

where the sums run over a square lattice, with $\langle \mathbf{i}, \mathbf{j} \rangle$ denoting nearest neighbors. Here we use the usual second quantization formalism, with $c_{\mathbf{i}, \sigma}$ ($c_{\mathbf{i}, \sigma}^\dagger$) being a fermionic operator that annihilates (creates) an electron with spin $\sigma = \uparrow, \downarrow$ on a given site \mathbf{i} ; $n_{\mathbf{i}, \sigma} = c_{\mathbf{i}, \sigma}^\dagger c_{\mathbf{i}, \sigma}$ is the fermion number operator. Similarly, $a_{\mathbf{i}}$ ($a_{\mathbf{i}}^\dagger$) is a bosonic operator that annihilates (creates) a phonon with energy $\hbar \omega_0$ on a given site \mathbf{i} . In the last term of Eq. (1), $\overleftrightarrow{\alpha}_{\mathbf{i}, \mathbf{j}} \equiv (\alpha_{\mathbf{i}, \mathbf{j}}^x, \alpha_{\mathbf{i}, \mathbf{j}}^y, 0)$ is the displacement tensor $\alpha_{\mathbf{i}, \mathbf{j}}^\nu \equiv i(\delta_{\mathbf{i}, \mathbf{j} + \alpha_\nu} - \delta_{\mathbf{i}, \mathbf{j} - \alpha_\nu})$, with α_ν being unitary translation in the ν direction, and $\overleftrightarrow{\sigma} \equiv (\sigma_x, \sigma_y, \sigma_z)$ are Pauli matrices related to electronic spin. The first two terms on the right-hand side of Eq. (1) correspond to the hopping of the electrons and their chemical potential, respectively. The third term describes the local harmonic oscillators,

while the fourth represents the EPC, with strength g . Finally, the last term is the RSOC, with strength t_R . We set the energy scale in units of the hopping integral t .

At this point, it is also worth mentioning that the ground state of the half-filled pure Holstein model ($t_R = 0$) is CDW for any EPC $g > 0$, due to instabilities from the van Hove singularity (vHs) and the Fermi surface nesting (FSN)^{33,44}. On the other hand, for a pure Rashba metal, i.e. $t_R \neq 0$ and $g = 0$, both FSN and vHs are absent at the half-filling, due to the splitting of the spin textures – similar to those presented in Fig. 1 (a) and (c). Such feature leads to no divergence in the density of states at the Fermi level $N(\omega = 0)$ – consequently, no divergence in the noninteracting electronic susceptibility. Therefore, within a weak coupling analysis of these two cases, one should expect that the RSOC must suppress CDW formation. Although this may be true for the weak coupling case, the scenario is less clear in the intermediate and strong coupling regimes, where the Fermi surface does not play a relevant role. In what follows, we investigate this problem at the ground state, by performing analyses within both MF and CPT approaches, fixing $\omega_0/t = 1$ while varying t_R and g .

III. MEAN-FIELD THEORY

We start by discussing the mean-field approach to the Rashba-Holstein Hamiltonian. To this end, we change the notation of Eq. (1), rewriting the phonon creation and annihilation operators in terms of position and momentum ones. For instance, by considering the pure Holstein model ($t_R = 0$), its Hamiltonian is

$$\begin{aligned} \mathcal{H}_H = & -t \sum_{\langle \mathbf{i}, \mathbf{j} \rangle, \sigma} (c_{\mathbf{i}, \sigma}^\dagger c_{\mathbf{j}, \sigma} + h.c.) - \mu \sum_{\mathbf{i}, \sigma} n_{\mathbf{i}, \sigma} \\ & - g \sqrt{\frac{2M\omega_0}{\hbar}} \sum_{\mathbf{i}, \sigma} n_{\mathbf{i}, \sigma}^\sigma \hat{X}_{\mathbf{i}} + \sum_{\mathbf{i}} \left(\frac{\hat{P}_{\mathbf{i}}^2}{2M} + \frac{M\omega_0^2}{2} \hat{X}_{\mathbf{i}}^2 \right), \end{aligned} \quad (2)$$

with $\hat{X}_{\mathbf{i}} = \sqrt{\frac{\hbar}{2M\omega_0}}(a_{\mathbf{i}} + a_{\mathbf{i}}^\dagger)$ and $\hat{P}_{\mathbf{i}} = i\sqrt{\frac{\hbar M\omega_0}{2}}(a_{\mathbf{i}}^\dagger - a_{\mathbf{i}})$ being the position and momentum operators, respectively, of a harmonic oscillator in a given site \mathbf{i} . Here, we define the mass of the harmonic oscillators (M) and the lattice constant as unities.

Within a static mean-field approach, we assume that the kinetic energy of lattice vibrations is negligible if compared with potential energy ($\hat{P}_{\mathbf{i}}^2/2M \ll M\omega_0^2 \hat{X}_{\mathbf{i}}^2/2$), i.e., we deal with a permanent distortion that breaks the translation symmetry of the lattice. This assumption corresponds to the adiabatic regime^{45,46}, i.e. $\omega_0 \rightarrow 0$ while keeping $M\omega_0^2 \equiv K$ finite. In this regime, the Hamiltonian is a quadratic form for electron creation/annihilation operators, therefore its ground state is exact by a mean-field approach.

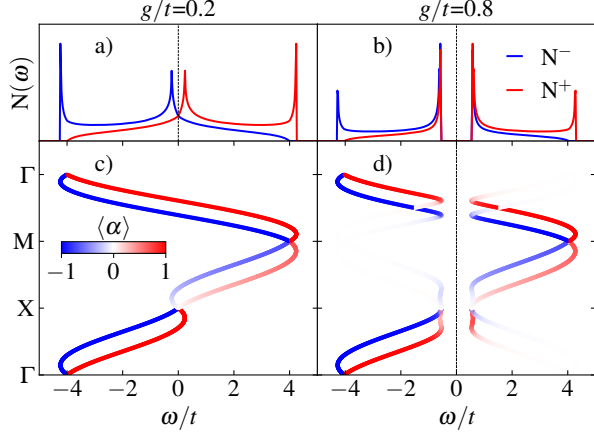


FIG. 1. The mean-field result for the density of states of the Rashba-Holstein model for EPC (a) $g/t = 0.2$, and (b) $g/t = 0.8$, and its electronic dispersion in (c) and (d), respectively. The results are for fixed RSOC $t_R/t = 0.5$, with the color codes indicating the chiral spin-texture polarization of bands.

Proceeding, we approximate the position operator by its expected value, assuming the *ansatz* $\hat{X}_i \rightarrow \langle X_i \rangle = X_0 + \cos(\mathbf{Q} \cdot \mathbf{i})X_1$, with $\mathbf{Q} = (\pi, \pi)$. Notice that other ansatzes involving arbitrary wavevectors $\mathbf{Q} = (q_x, q_y)$ can be explored, even in incommensurate cases⁴⁷. However, owing to the four-fold rotational symmetry inherent to the square lattice, along with the nesting properties and the commensurate filling, it is expected that the (π, π) configuration is the one that most significantly reduces the internal energy. Therefore, the MF Holstein Hamiltonian becomes

$$\begin{aligned} \mathcal{H}_H = & -t \sum_{\langle \mathbf{i}, \mathbf{j} \rangle, \sigma} (c_{\mathbf{i}, \sigma}^\dagger c_{\mathbf{j}, \sigma} + \text{H.c.}) - \mu \sum_{\mathbf{i}, \sigma} n_{\mathbf{i}, \sigma} \\ & - g \sqrt{\frac{2M\omega_0}{\hbar}} \sum_{\mathbf{i}, \sigma} n_{\mathbf{i}, \sigma} [X_0 + X_1 \cos(\mathbf{Q} \cdot \mathbf{i})] \\ & + \frac{NM\omega_0^2}{2} (X_0^2 + X_1^2), \end{aligned} \quad (3)$$

where N is the number of lattice sites.

The inclusion of the Rashba term changes the electron dispersion, and the eventual mean-field Hamiltonian in reciprocal space reads

$$\begin{aligned} \mathcal{H}_{MF} = & \sum_{\mathbf{k}, \sigma} (\varepsilon_{\mathbf{k}} - \mu') c_{\mathbf{k}\sigma}^\dagger c_{\mathbf{k}\sigma} + \sum_{\mathbf{k}, \sigma, \sigma'} (\hat{V}_{\mathbf{k}})_{\sigma\sigma'} c_{\mathbf{k}\sigma}^\dagger c_{\mathbf{k}\sigma'}, \\ & - g \sqrt{\frac{M\omega_0}{2\hbar}} X_1 \sum_{\mathbf{k}, \sigma} (c_{\mathbf{k}+\mathbf{Q}\sigma}^\dagger c_{\mathbf{k}\sigma} + \text{H.c.}) \\ & + \frac{NM\omega_0^2}{2} (X_0^2 + X_1^2), \end{aligned} \quad (4)$$

with $\varepsilon_{\mathbf{k}} = -2t(\cos k_x + \cos k_y)$, $\hat{V}_{\mathbf{k}} \equiv 2t_R(\sigma_x \sin k_y - \sigma_y \sin k_x)$, and $\mu' = \mu + g\sqrt{2M\omega_0/\hbar}X_0$. In a basis of

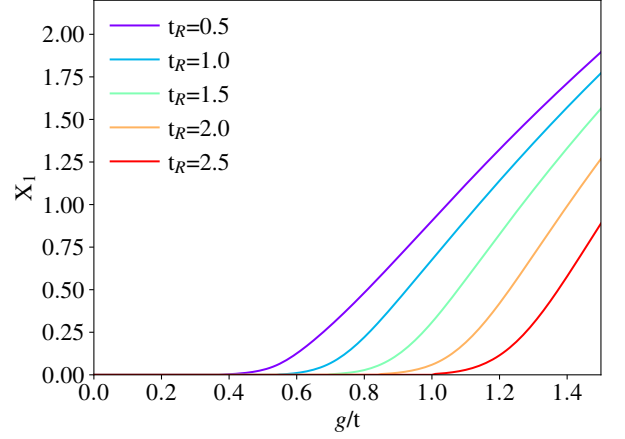


FIG. 2. The behavior of the ground state mean-field parameter X_1 (proportional to the CDW order parameter) as a function of the electron-phonon coupling g , for different values of RSOC t_R 's.

Nambu spinors $\Phi_{\mathbf{k}}^\dagger = (c_{\mathbf{k}\uparrow}^\dagger, c_{\mathbf{k}\downarrow}^\dagger, c_{\mathbf{k}+\mathbf{Q}\uparrow}^\dagger, c_{\mathbf{k}+\mathbf{Q}\downarrow}^\dagger)$, we obtain a quadratic form representation of \mathcal{H}_{MF} ,

$$\mathcal{H}_{MF} = \frac{1}{2} \sum_{\mathbf{k}} \Phi_{\mathbf{k}}^\dagger \hat{H}_{\mathbf{k}} \Phi_{\mathbf{k}} + \frac{NM\omega_0^2}{2} (X_0^2 + X_1^2) \quad (5)$$

where

$$\hat{H}_{\mathbf{k}} = \begin{pmatrix} \varepsilon_{\mathbf{k}} - \mu' & (\hat{V}_{\mathbf{k}})_{\uparrow\downarrow} & -\Delta X & 0 \\ (\hat{V}_{\mathbf{k}})_{\downarrow\uparrow} & \varepsilon_{\mathbf{k}} - \mu' & 0 & -\Delta X \\ -\Delta X & 0 & \varepsilon_{\mathbf{k}+\mathbf{Q}} - \mu' & (\hat{V}_{\mathbf{k}+\mathbf{Q}})_{\uparrow\downarrow} \\ 0 & -\Delta X & (\hat{V}_{\mathbf{k}+\mathbf{Q}})_{\downarrow\uparrow} & \varepsilon_{\mathbf{k}+\mathbf{Q}} - \mu' \end{pmatrix} \quad (6)$$

with $\Delta X = g\sqrt{2M\omega_0/\hbar}X_1$. Notice that we added X_0 to the chemical potential μ' , since this field shifts the energy level, while the X_1 field modulates the electronic distribution, therefore being proportional to the amplitude of the CDW order parameter.⁴⁸

The parameters $X_{0(1)}$ are determined self-consistently by minimizing the Helmholtz free energy, through the diagonalization of Eq. (5). We use the minimization solutions to describe the ground state properties of the system, such as the density of state (DOS) and the electron dispersion, e.g., as displayed in Fig. 1 for small and large values of EPC, while keeping $t_R/t = 0.5$ fixed. As presented in Figs. 1(a) and (c), when $g/t = 0.2$, the RSOC splits the electronic spectra into two branches with well-defined chiralities, $\langle \hat{\sigma} \rangle \cdot (\mathbf{k} \times \hat{z})/|\mathbf{k}| = \pm 1$ for right-handed and left-handed. Such a split shifts the energy levels and, consequently, the van Hove singularities, leading to a reduction in the DOS at the half-filling, as shown in Fig. 1(a). On the other hand, for large EPC, a CDW phase emerges and creates a charge gap at the half-filling, as displayed in Figs. 1(b) and (d), for $g/t = 0.8$. This result provides a few hints that the RSOC is harmful to the CDW phase.

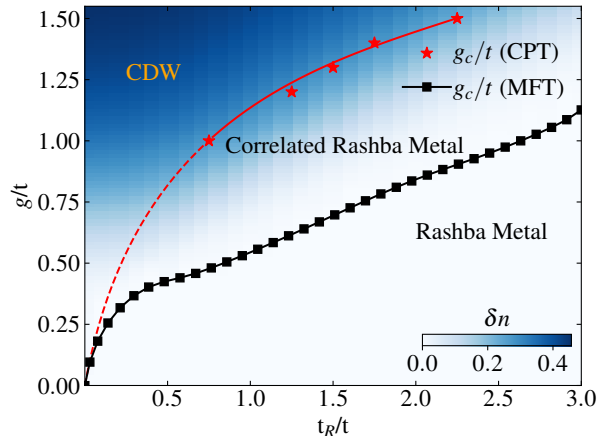


FIG. 3. The ground-state phase diagram of Holstein-Rashba model in the half-filled square lattice. The black square symbols correspond to the mean-field solution, while the red star ones denote the CPT results. The blue heatmap indicates the amplitude of charge modulation in the CDW phase for the MFT solution. The red curve is just a guide to the eye.

To further emphasize the effects of the RSOC on the CDW phase, Fig. 2 displays the behavior of X_1 as a function of g/t , for different spin-orbit couplings, in the ground state. For fixed values of g/t , where the minimization of the energy leads to CDW, it is clear that the main effect of the RSOC is to reduce X_1 , which is deleterious to charge modulation. At this point, a remark should be made: the asymptotic behavior to X_1 as a function of g/t may be an artifact of the mean-field solution. Then, we define $X_1 = 10^{-3}$ as the lower bound limit for the CDW phase, which is enough to reproduce $g_c \rightarrow 0$ when $t_R \rightarrow 0$, as expected for the pure Holstein model at the half-filled square lattice. This lower bound limit defines the critical region where the CDW phase is destroyed (or emerges).

Repeating similar analyses as those of Fig. 2, we are able to present the mean-field phase diagram of the Rashba-Holstein model at half-filling, as shown in Fig. 3. Here, the CDW and Rashba metal phases are separated by the curve going through the black squares, while the color-map scheme describes the amplitude of the CDW charge modulation, δn . As complementary information, Fig. 4 displays the critical CDW temperature T_{CDW} , below which the system opens a gap⁴⁹. In line with the previous discussion, the RSOC tends to suppress the CDW phase, decreasing both the critical temperatures and the order parameter, eventually leading to a Rashba metal.

Despite being obtained by a static mean-field approach, the phase diagram of Fig. 3 is expected to provide the correct transition lines when $\omega_0 \rightarrow 0$. However, $\omega_0/t = 1$ is clearly away from this limit, which may require less biased methodologies to investigate the Hamiltonian properties, as discussed in the next Section.

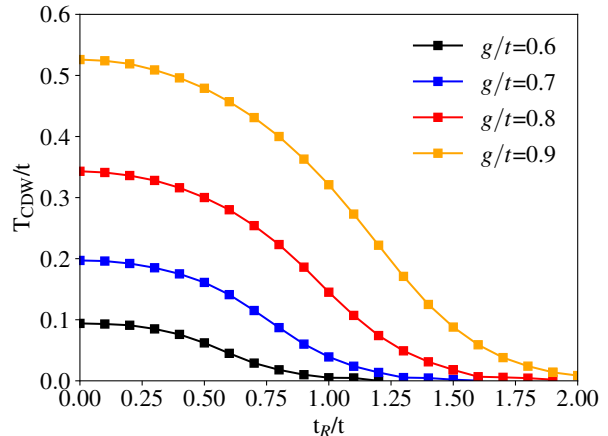


FIG. 4. CDW critical temperature as a function of t_R/t for different values of g/t .

IV. CLUSTER PERTURBATION THEORY

Now, we use the cluster perturbation theory, which is a convenient technique to extract spectral weights and the electronic DOS of a correlated system. Briefly speaking, the CPT consists of partitioning an infinite lattice into clusters of finite size where the Hamiltonian is exactly solved, while coupling the clusters by perturbation theory approaches. A pedagogical introduction to this method can be found in Ref. 50–53.

Within this approach, we decompose the Hamiltonian as

$$H = H_{\text{cluster}} + T, \quad (7)$$

where $H_{\text{cluster}} = K + H_{\text{int}}$ describes the operations inside a given finite-sized cluster, with $K = \sum_{\alpha,\beta} t_{\alpha,\beta} c_{\alpha}^{\dagger} c_{\beta}$ and $H_{\text{int}} = -g \sum_{\mathbf{i},\sigma} n_{\mathbf{i},\sigma} (a_{\mathbf{i}} + a_{\mathbf{i}}^{\dagger})$ being the hopping and the EPC terms, respectively. The term $T = \sum_{\alpha,\beta} V_{\alpha,\beta} c_{\alpha}^{\dagger} c_{\beta}$ is the one that connects different clusters of the superlattice (i.e., intercluster sites). Given this, one can write the Green's functions as

$$\mathbf{G}(\omega)^{-1} = \mathbf{G}'(\omega)^{-1} - \mathbf{V}, \quad (8)$$

where $\mathbf{G}(\omega)$ and $\mathbf{G}'(\omega)$ are the infinite lattice and the (exact) finite-sized cluster Green's functions, respectively. As the cluster superlattice has a reduced Brillouin zone, one can connect any wavevector \mathbf{k} of the original Brillouin zone to a wavevector $\tilde{\mathbf{k}}$ in the reduced one by $\mathbf{k} = \tilde{\mathbf{k}} + \mathbf{K}$, where \mathbf{K} is an element of the reciprocal superlattice. Therefore, in the reduced Brillouin zone, Eq. (8) is given by

$$\mathbf{G}(\tilde{\mathbf{k}}, \omega)^{-1} = \mathbf{G}'(\omega)^{-1} - \mathbf{V}(\tilde{\mathbf{k}}), \quad (9)$$

which eventually leads to the CPT Green's functions

$$G_{\text{CPT}}(\mathbf{k}, \omega) = \frac{1}{L} \sum_{a,b} e^{-i\mathbf{k}(\mathbf{r}_a - \mathbf{r}_b)} G_{a,b}(\tilde{\mathbf{k}}, \omega), \quad (10)$$

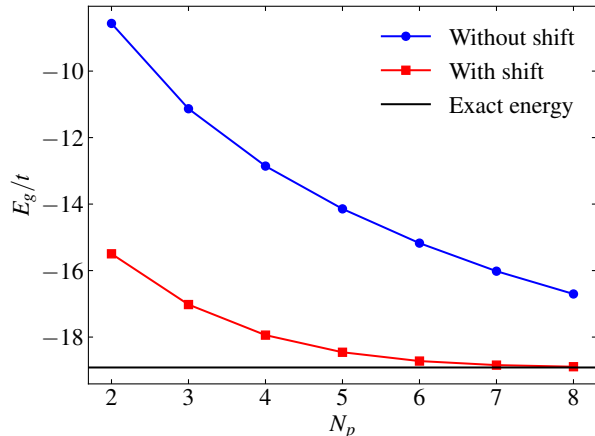


FIG. 5. The ground state energy of the Holstein model for $g/t = 1.5$, in a 2×2 plaquette, as a function of the cutoff number of phonons per site N_p . The red squares (blue circles) symbols denote the ground state energies for the case with (without) a shift to symmetrize the electron-phonon term.

with $\mathbf{r}_{a(b)}$ being the position of the intra-cluster sites.

The CPT Green's functions take into account the leading order in the interaction term, and allow one to obtain the spectral weight

$$A_0(\mathbf{k}, \omega) = -\frac{1}{2\pi} \text{Im}[G_{\text{CPT}}(\mathbf{k}, \omega)], \quad (11)$$

and the DOS

$$N(\omega) = \frac{1}{N} \sum_{\mathbf{k}} A_0(\mathbf{k}, \omega). \quad (12)$$

In what follows, we use the DOS to identify the transition from a gapped CDW phase to a Rashba metal.

At this point, it is worth discussing a few technical issues about our CPT implementation. Due to the phonon degrees of freedom, the Hilbert space is infinite, which demands a cutoff in the total number of phonons to perform the exact diagonalization procedure. Among the different ways of establishing this cutoff, we have defined a maximum limit, N_p , for the number of phonons per site. Its value is determined through a systematic analysis of the ground state energy E_g as a function of N_p , as displayed in Fig. 5, for fixed $g/t = 1.5$ and $\omega_0/t = 1$, in a 2×2 plaquette. Notice that $E_g(N_p)$ goes asymptotically to the limit $N_p \rightarrow \infty$, so the error from the cut-off may be disregarded for a given value of N_p . However, the electron-phonon term described in Eq. (1) requires a substantial number of phonons to attain the correct ground state, as evidenced by the behavior of the blue circle symbols in Fig. 5. To circumvent this difficulty and keep N_p as small as possible, we perform a shift in the phonon operators $a_i \rightarrow (a_i + g\langle n \rangle)$, with $\langle n \rangle$ being the average electron density. We emphasize that such a shift is equivalent to a change in the origin of the phonon position operators \hat{X}_i to deal just with excitations around

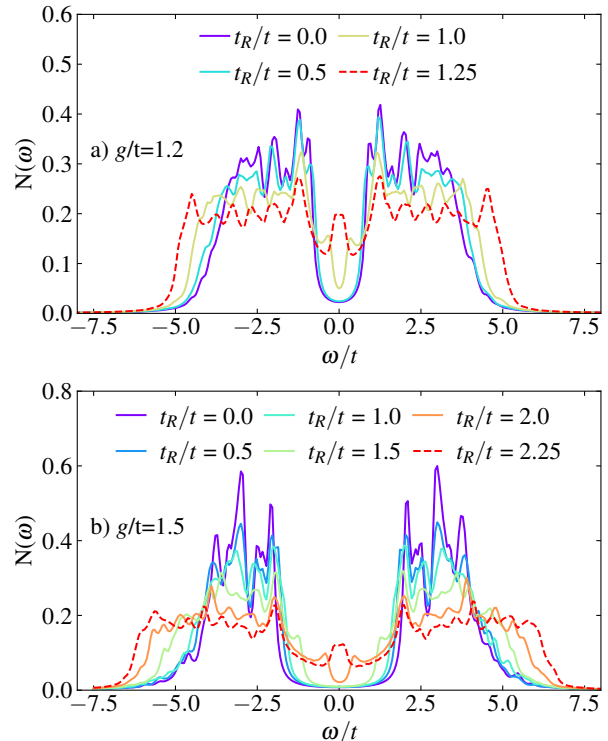


FIG. 6. The DOS of the Rashba-Holstein model for EPC (a) $g/t = 1.2$ and (b) $g/t = 1.5$, for different values of RSOC t_R .

its mean value. This drastically reduces the number of required phonons, as shown by the behavior of the red square symbols in Fig. 5. Despite this improvement, the greater the EPC, the larger the values of N_p , therefore we limit our analyses to intermediate coupling strengths for clusters of 2×2 sites.

Now, using the CPT method we turn to discuss the effects of the RSOC on the spectral properties of our charge-ordered system, for fixed $\omega_0/t = 1$, and at half-filling. Figure 6(a) displays the behavior of $N(\omega)$ for $g/t = 1.2$ and different values of t_R . When $t_R = 0$, the system has a large charge gap around $\omega = 0$, in line with our expectation of a CDW phase for the Holstein model in the half-filled square lattice. Interestingly, the size of the gap remains nearly unchanged for $t_R/t \lesssim 0.5$, which shows that the CDW phase is robust against spin-orbit perturbations. However, for larger RSOC, the charge gap drastically decreases, until $N(\omega \approx 0)$ exhibits a peak instead of a gap for $t_R/t \approx 1.25$. This specific change in the behavior of $N(\omega)$ around $\omega \approx 0$ (and $t_R/t \approx 1.25$) is a clear indication of the occurrence of a phase transition from the CDW phase to a Rashba metal.

A very similar behavior occurs for different values of g , as displayed in Fig. 6(b), for $g/t = 1.5$. The main difference between this case and the previous one is the need for a larger RSOC to destroy the charge gap. In view of this, here we define as *critical points* the values of t_R at which $N(\omega)$ exhibits a peak instead of a gap at

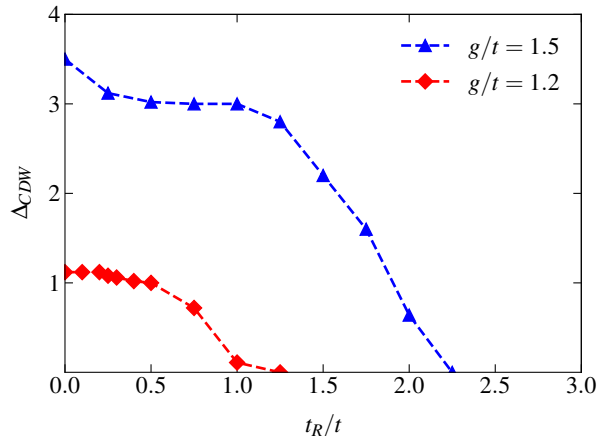


FIG. 7. The CDW charge gap, Δ_{CDW} as a function of the RSOC, t_R/t , for fixed $\omega_0/t = 1$.

the half-filling. These CPT critical points are presented as red star symbols in the phase diagram of Fig. 3, with the red (dashed and solid) lines being just guides to the eye.

In order to further emphasize the phase transitions, we extract the charge gap directly from Fig. 6 by defining the CDW order parameter, Δ_{CDW} , as the energy difference between the two peaks away from $\omega = 0$. The behavior of Δ_{CDW} as a function of t_R is displayed in Fig. 7, for $g/t = 1.2$ (red diamond symbols) and 1.5 (blue triangle symbols), from which one may notice that the gap closing is consistent with a second order phase transition. In particular, the suppression of the CDW phase seems to occur at $t_{R(c)} = 1.1 \pm 0.1$ for $g/t = 1.2$, and at $t_{R(c)} = 2.1 \pm 0.1$ for $g/t = 1.5$.

There are clear differences between the CPT and MFT results, which may be understood through two key remarks. First, and foremost, the CPT method takes into account the effects of short-range electronic correlations, while the MFT deals with local ones. That is, the MFT exhibits the points where the Rashba metal becomes on-site correlated, while the CPT provides insights when these correlations become long-ranged. Therefore, the region enclosed between the MFT and CPT lines in Fig. 3 defines a *correlated* Rashba metal, i.e. metallic (from CPT) but with on-site correlations (from MFT approach). As a second remark, we recall that the mean-field solution is exact at the ground state when $\omega_0 \rightarrow 0$, thus the MFT line in Fig. 3 can also be interpreted as as the boundary of the adiabatic limit. That is, if one reduces ω_0 , the CPT transition line must be pushed into the MFT ones. Then, it provides the behavior of the critical points when ω_0 changes.

At this point, it is worth discussing the emergence of pairing correlations in the absence of the CDW ones. As the occurrence of superconductivity is a challenge for both methodologies, we analyze the *s*-wave pair corre-

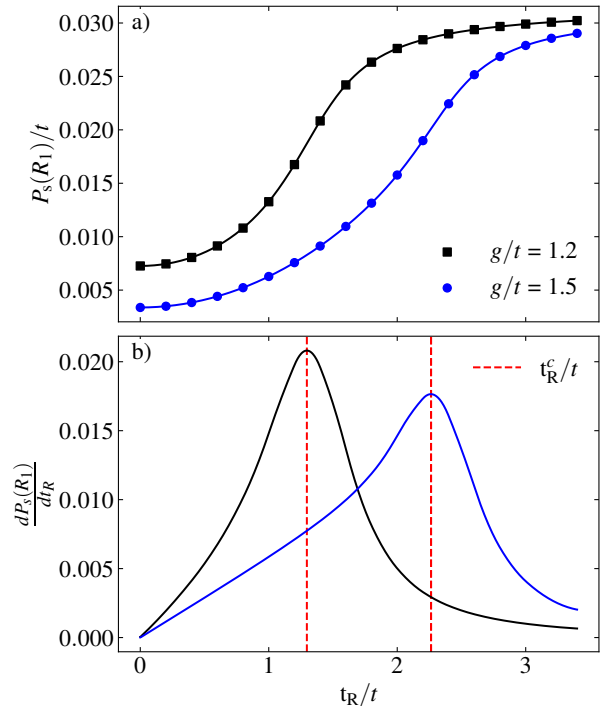


FIG. 8. The *s*-wave pair correlation function $P_s(\mathbf{i}, \mathbf{j})$ as a function of RSOC and its numerical derivative $dP_s(\mathbf{i}, \mathbf{j})/dt_R$ for two values of EPC. The correlation function is calculated between pairs at a site \mathbf{i} and its nearest-neighbor \mathbf{j} symbolized here by $(\mathbf{i}, \mathbf{j}) = (R_1)$.

lation functions⁵⁴

$$P_s(\mathbf{i}, \mathbf{j}) = \frac{1}{2} \langle b_{\mathbf{i}}^\dagger b_{\mathbf{j}} + \text{H.c.} \rangle \quad (13)$$

with $b_{\mathbf{i}}^\dagger = c_{\mathbf{i}\uparrow}^\dagger c_{\mathbf{i}\downarrow}^\dagger$ ($b_{\mathbf{j}} = c_{\mathbf{j}\downarrow} c_{\mathbf{j}\uparrow}$), restricting our analysis to nearest-neighbor sites. This function is computed in real space, after partitioning the system in the cluster scheme described above. Figure 8(a) presents $P_s(|\mathbf{i} - \mathbf{j}| = 1)$ as a function of t_R for $g/t = 1.2$ and 1.5 , from which we see an enhancement of the pairing correlations. This result provides us with an interesting feature: the derivative of the nearest-neighbor pair correlation function (dP_s/dt_R) exhibits peaks for values very close to the CDW critical points, as shown in Fig. 8(b). Such a behavior is not a coincidence; as charge-charge correlations compete with pairing ones, then it is expected that $P_s(\mathbf{i}, \mathbf{j})$ should be enhanced around the points where the CDW gap closes, independently whether the ground state is superconducting or not. Therefore, although this result is not enough to support the existence of superconductivity, it reinforces our previous findings about the nature of the charge gap being a CDW phase, and about the location of the CPT critical points presented in the phase diagram of Fig. 3.

Last, but not least, we recall that the spin-orbit coupling has been investigated in different contexts of strongly correlated systems, in particular for those involving electron-electron interactions. Then, it is im-

perative to compare these cases with ours, highlighting both their similarities and differences. For instance, for the repulsive Hubbard model in the half-filled square lattice, the inclusion of the RSOC leads to the emergence of novel magnetic phases, which may include spiral and striped ones; away from the half-filling, ferromagnetism may appear^{55–60}. This occurs due to the spin-flip term in the RSOC, which disfavors the staggered antiferromagnetic ground state of the half-filling, suppressing the charge gap, while keeping gapless spin excitations. Due to the spin dependence in the interaction term in the Hubbard model, the CPT spectral properties for this case exhibit a clear dependence of the chiral bands and DOS as a function of the Hubbard interaction strength U ⁵⁶. It is substantially different from our present study, since the interaction term in the Rashba-Holstein model is not spin-dependent, with the spin and charge gaps emerging/disappearing together. Furthermore, noteworthy changes manifest in the attractive Hubbard model when subjected to the RSOC. This model exhibits s -wave superconductivity for any filling^{54,61,62}, whose critical temperatures are significantly increased with the inclusion of the RSOC^{63–65}. This enhancement results from the suppression of charge-charge correlations, in line with our findings for the Rashba-Holstein model. Given that the antiadiabatic regime ($\omega_0 \rightarrow \infty$) of the Holstein one can be mapped onto the attractive Hubbard model, we anticipate the emergence of superconductivity in our scenario. However, achieving this would require the application of unbiased methodologies, such as quantum Monte Carlo methods, which is beyond the scope of the present study.

V. CONCLUSIONS

In this work, we have studied the impact of the Rashba spin-orbit coupling to a charge-ordered system, as the Holstein model. To this end, we investigated the Rashba-Holstein model using two methodologies: (i) a static

mean-field approach, and (ii) the cluster perturbation theory – the latter provides the spectral functions of an infinite system with short-range correlations, i.e. beyond a Hartree-Fock approximation. Given this, our main findings are summarized in the phase diagram of Fig. 3, which presents the CPT and MFT results, from which one notices that the RSOC is harmful to the CDW phase. This deleterious feature of the RSOC could be understood from the diminishing DOS at the half-filling when t_R increases, from a weak coupling point-of-view; or by a large energetic price to pay to avoid spin-flip processes (within the CDW phase), from a strong coupling point-of-view. Furthermore, as shown in Figs. 6 and 7, the transition from the CDW phase to a *correlated* Rashba metal seems to be continuous, with the transition line being pushed to larger values of t_R when $\omega_0 \rightarrow 0$. Even though the critical phenomena properties (such as critical exponents) are beyond the scope of this work, our phase diagram $g \times t_R$ provides accurate critical points, whose fundamental properties may shed light into the growing class of Rashba materials^{26–28}.

ACKNOWLEDGMENTS

The authors are grateful to R.R. dos Santos for enlightening discussions and suggestions. Financial support from Fundação Carlos Chagas Filho de Amparo à Pesquisa do Estado do Rio de Janeiro, grant number E-26/200.258/2023 - SEI-260003/000623/2023 (N.C.C.); and from CNPq grant number 313065/2021-7 (N.C.C.) is gratefully acknowledged. We also acknowledge support from INCT-IQ. T.P.C. acknowledge support from CAPES (Brazil). S.A.S.Jr. acknowledges support from CNPq (Brazil) and Fundação Carlos Chagas Filho de Amparo à Pesquisa do Estado do Rio de Janeiro process SEI-260003/006232/2023. R.A.F. acknowledges support from Fundação Carlos Chagas Filho de Amparo à Pesquisa do Estado do Rio de Janeiro and CNPq (Brazil).

¹ Rubén Mas-Ballesté, Cristina Gómez-Navarro, Julio Gómez-Herrero, and Félix Zamora, “2D materials: to graphene and beyond,” *Nanoscale* **3**, 20–30 (2011).

² Ankur Gupta, Tamilselvan Sakthivel, and Sudipta Seal, “Recent development in 2D materials beyond graphene,” *Progress in Materials Science* **73**, 44–126 (2015).

³ K. S. Novoselov, A. Mishchenko, A. Carvalho, and A. H. Castro Neto, “2D materials and van der Waals heterostructures,” *Science* **353**, aac9439 (2016), <https://www.science.org/doi/pdf/10.1126/science.aac9439>.

⁴ Ethan C Ahn, “2D materials for spintronic devices,” *npj 2D Materials and Applications* **4**, 17 (2020).

⁵ Valeri N. Kotov, Bruno Uchoa, Vitor M. Pereira, F. Guinea, and A. H. Castro Neto, “Electron-Electron Interactions in Graphene: Current Status and Perspectives,” *Rev. Mod. Phys.* **84**, 1067–1125 (2012).

⁶ Y.-X. Zhang, W.-T. Chiu, N. C. Costa, G. G. Batrouni, and R. T. Scalettar, “Charge Order in the Holstein Model on a Honeycomb Lattice,” *Phys. Rev. Lett.* **122**, 077602 (2019).

⁷ Thereza Paiva, R. T. Scalettar, W. Zheng, R. R. P. Singh, and J. Oitmaa, “Ground-state and finite-temperature signatures of quantum phase transitions in the half-filled Hubbard model on a honeycomb lattice,” *Phys. Rev. B* **72**, 085123 (2005).

⁸ A. H. Castro Neto, F. Guinea, N. M. R. Peres, K. S. Novoselov, and A. K. Geim, “The electronic properties of graphene,” *Rev. Mod. Phys.* **81**, 109–162 (2009).

⁹ Yuan Cao, Valla Fatemi, Shiang Fang, Kenji Watanabe, Takashi Taniguchi, Efthimios Kaxiras, and Pablo Jarillo-Herrero, “Unconventional superconductivity in magic-angle graphene superlattices,” *Nature* **556**, 43–50 (2018).

- ¹⁰ Cheng Gong, Lin Li, Zhenglu Li, Huiwen Ji, Alex Stern, Yang Xia, Ting Cao, Wei Bao, Chenzhe Wang, Yuan Wang, Z. Q. Qiu, R. J. Cava, Steven G. Louie, Jing Xia, and Xiang Zhang, “Discovery of intrinsic ferromagnetism in two-dimensional van der Waals crystals,” *Nature* **546**, 265–269 (2017).
- ¹¹ Bevin Huang, Genevieve Clark, Efrén Navarro-Moratalla, Dahlia R. Klein, Ran Cheng, Kyle L. Seyler, Ding Zhong, Emma Schmidgall, Michael A. McGuire, David H. Cobden, Wang Yao, Di Xiao, Pablo Jarillo-Herrero, and Xiaodong Xu, “Layer-dependent ferromagnetism in a van der Waals crystal down to the monolayer limit,” *Nature* **546**, 270–273 (2017).
- ¹² S. Manzeli, D. Ovchinnikov, D. Pasquier, O.V. Yazyev, and A. Kis, “2D transition metal dichalcogenides,” *Nature Reviews Materials* **2**, 17033 (2017).
- ¹³ G. Grüner, “The dynamics of charge-density waves,” *Rev. Mod. Phys.* **60**, 1129–1181 (1988).
- ¹⁴ L. P. Gor’kov and G. Grüner, *Charge density waves in solids* (Elsevier, Amsterdam, 1989).
- ¹⁵ Katsuki Sugawara, Yuki Nakata, Ryota Shimizu, Patrick Han, Taro Hitosugi, Takafumi Sato, and Takashi Takahashi, “Unconventional Charge-Density-Wave Transition in Monolayer 1T-TiSe₂,” *ACS Nano* **10**, 1341–1345 (2015).
- ¹⁶ Dongjing Lin, Shichao Li, Jinsheng Wen, Helmuth Berger, László Forró, Huibin Zhou, Shuang Jia, Takashi Taniguchi, Kenji Watanabe, Xiaoxiang Xi, and Mohammad Saeed Bahramy, “Patterns and driving forces of dimensionality-dependent charge density waves in 2H-type transition metal dichalcogenides,” *Nature Communications* **11**, 2406 (2020).
- ¹⁷ Yizhi Ge and Amy Y. Liu, “Effect of dimensionality and spin-orbit coupling on charge-density-wave transition in 2H-TaSe₂,” *Phys. Rev. B* **86**, 104101 (2012).
- ¹⁸ Chao-Sheng Lian, Christoph Heil, Xiaoyu Liu, Chen Si, Feliciano Giustino, and Wenhui Duan, “Intrinsic and doping-enhanced superconductivity in monolayer 1H-TaS₂: Critical role of charge ordering and spin-orbit coupling,” *Phys. Rev. B* **105**, L180505 (2022).
- ¹⁹ Junsaku Nitta, Tatsushi Akazaki, Hideaki Takayanagi, and Takatomo Enoki, “Gate Control of Spin-Orbit Interaction in an Inverted In_{0.53}Ga_{0.47}As/In_{0.52}Al_{0.48}As Heterostructure,” *Phys. Rev. Lett.* **78**, 1335–1338 (1997).
- ²⁰ Christian R. Ast, Jürgen Henk, Arthur Ernst, Luca Moreschini, Mihaela C. Falub, Daniela Pacilé, Patrick Bruno, Klaus Kern, and Marco Grioni, “Giant Spin Splitting through Surface Alloying,” *Phys. Rev. Lett.* **98**, 186807 (2007).
- ²¹ Eli Rotenberg, J. W. Chung, and S. D. Kevan, “Spin-Orbit Coupling Induced Surface Band Splitting in Li/W(110) and Li/Mo(110),” *Phys. Rev. Lett.* **82**, 4066–4069 (1999).
- ²² S. LaShell, B. A. McDougall, and E. Jensen, “Spin Splitting of an Au(111) Surface State Band Observed with Angle Resolved Photoelectron Spectroscopy,” *Phys. Rev. Lett.* **77**, 3419–3422 (1996).
- ²³ Hongki Min, J. E. Hill, N. A. Sinitsyn, B. R. Sahu, Leonard Kleinman, and A. H. MacDonald, “Intrinsic and Rashba spin-orbit interactions in graphene sheets,” *Phys. Rev. B* **74**, 165310 (2006).
- ²⁴ Tarik P. Cysne, Aires Ferreira, and Tatiana G. Rappoport, “Crystal-field effects in graphene with interface-induced spin-orbit coupling,” *Phys. Rev. B* **98**, 045407 (2018).
- ²⁵ Tarik P. Cysne, Jose H. Garcia, Alexandre R. Rocha, and Tatiana G. Rappoport, “Quantum Hall effect in graphene with interface-induced spin-orbit coupling,” *Phys. Rev. B* **97**, 085413 (2018).
- ²⁶ Paul Z. Hanakata, A. S. Rodin, Alexandra Carvalho, Harold S. Park, David K. Campbell, and A. H. Castro Neto, “Two-dimensional square buckled Rashba lead chalcogenides,” *Phys. Rev. B* **96**, 161401 (2017).
- ²⁷ Paul Z. Hanakata, A. S. Rodin, Harold S. Park, David K. Campbell, and A. H. Castro Neto, “Strain-induced gauge and Rashba fields in ferroelectric Rashba lead chalcogenide PbX monolayers ($X = S, Se, Te$),” *Phys. Rev. B* **97**, 235312 (2018).
- ²⁸ Jiajia Chen, Kai Wu, Wei Hu, and Jinlong Yang, “Spin-Orbit Coupling in 2D Semiconductors: A Theoretical Perspective,” *The Journal of Physical Chemistry Letters* **12**, 12256–12268 (2021).
- ²⁹ D. Pesin and L. Balents, “Mott physics and band topology in materials with strong spin-orbit interaction,” *Nature Physics* **6**, 376–381 (2010).
- ³⁰ W. Witczak-Krempa, G. Chen, Y.B. Kim, and L. Balents, “Correlated quantum phenomena in the strong spin-orbit regime,” *Annual Review of Condensed Matter Physics* **5**, 57–82 (2014).
- ³¹ J.G. Rau, E.K.-H. Lee, and H.-Y. Kee, “Spin-orbit physics giving rise to novel phases in correlated systems: Iridates and related materials,” *Annual Review of Condensed Matter Physics* **7**, 195–221 (2016).
- ³² T Holstein, “Studies of polaron motion,” *Annals of Physics* **8**, 325–342 (1959).
- ³³ Natanael C. Costa, Kazuhiro Seki, Seiji Yunoki, and Sandro Sorella, “Phase diagram of the two-dimensional Hubbard-Holstein model,” *Communications Physics* **3**, 80 (2020).
- ³⁴ P. M. Dee, K. Nakatsukasa, Y. Wang, and S. Johnston, “Temperature-filling phase diagram of the two-dimensional Holstein model in the thermodynamic limit by self-consistent Migdal approximation,” *Phys. Rev. B* **99**, 024514 (2019).
- ³⁵ Owen Bradley, George G. Batrouni, and Richard T. Scalettar, “Superconductivity and charge density wave order in the two-dimensional Holstein model,” *Phys. Rev. B* **103**, 235104 (2021).
- ³⁶ B. Cohen-Stead, N. C. Costa, E. Khatami, and R. T. Scalettar, “Effect of strain on charge density wave order in the Holstein model,” *Phys. Rev. B* **100**, 045125 (2019).
- ³⁷ Maykon V. Araújo, José P. de Lima, Sandro Sorella, and Natanael C. Costa, “Two-dimensional $t - t'$ Holstein model,” *Phys. Rev. B* **105**, 165103 (2022).
- ³⁸ Shaozhi Li, E. A. Nowadnick, and S. Johnston, “Quasiparticle properties of the nonlinear Holstein model at finite doping and temperature,” *Phys. Rev. B* **92**, 064301 (2015).
- ³⁹ Philip M. Dee, Jennifer Coulter, Kevin G. Kleiner, and Steven Johnston, “Relative importance of nonlinear electron-phonon coupling and vertex corrections in the Holstein model,” *Communications Physics* **3**, 145 (2020).
- ⁴⁰ G. Paleri, F. Hébert, B. Cohen-Stead, K. Barros, RT. Scalettar, and G. G. Batrouni, “Quantum Monte Carlo study of an anharmonic Holstein model,” *Phys. Rev. B* **103**, 195117 (2021).
- ⁴¹ B. Xiao, N. C. Costa, E. Khatami, G. G. Batrouni, and R. T. Scalettar, “Charge density wave and superconductivity in the disordered Holstein model,” *Phys. Rev. B* **103**,

- L060501 (2021).
- ⁴² Sebastião dos Anjos Sousa-Júnior, Raimundo R. dos Santos, and Natanael C. Costa, “Magnetic impurities in a charge-ordered background,” *Phys. Rev. B* **107**, 075140 (2023).
- ⁴³ N. C. Costa, T. Blommel, W.-T. Chiu, G. Batrouni, and R. T. Scalettar, “Phonon Dispersion and the Competition between Pairing and Charge Order,” *Phys. Rev. Lett.* **120**, 187003 (2018).
- ⁴⁴ M. Hohenadler and G. G. Batrouni, “Dominant charge density wave correlations in the Holstein model on the half-filled square lattice,” *Phys. Rev. B* **100**, 165114 (2019).
- ⁴⁵ Zhou Li, D. Baillie, C. Blois, and F. Marsiglio, “Ground-state properties of the Holstein model near the adiabatic limit,” *Phys. Rev. B* **81**, 115114 (2010).
- ⁴⁶ A. S. Alexandrov, V. V. Kabanov, and D. K. Ray, “From electron to small polaron: An exact cluster solution,” *Phys. Rev. B* **49**, 9915–9923 (1994).
- ⁴⁷ Nei Lopes, Daniel Reyes, Natanael C. Costa, Mucio A. Continentino, and Christopher Thomas, “Incommensurate charge density wave in multiband intermetallic systems exhibiting competing orders,” *Phys. Rev. B* **107**, 205141 (2023).
- ⁴⁸ Indeed, if we define $\langle n_i \rangle = n + \cos(\mathbf{Q} \cdot \mathbf{i})\delta n$, from Eq. (3) one obtains $\delta n = \omega_0 \sqrt{\frac{M\hbar\omega_0}{2} \frac{X_1}{g}}$.
- ⁴⁹ Again, notice that tail-like behavior of T_{CDW} for large SOC is a mean-field artifact.
- ⁵⁰ Martin Hohenadler, Markus Aichhorn, and Wolfgang von der Linden, “Spectral function of electron-phonon models by cluster perturbation theory,” *Phys. Rev. B* **68**, 184304 (2003).
- ⁵¹ David Sénéchal, Danny Perez, and Dany Plouffe, “Cluster perturbation theory for Hubbard models,” *Phys. Rev. B* **66**, 075129 (2002).
- ⁵² D. Sénéchal, D. Perez, and M. Pioro-Ladrière, “Spectral Weight of the Hubbard Model through Cluster Perturbation Theory,” *Phys. Rev. Lett.* **84**, 522–525 (2000).
- ⁵³ David Sénéchal, “An introduction to quantum cluster methods,” (2010), [arXiv:0806.2690 \[cond-mat.str-el\]](https://arxiv.org/abs/0806.2690).
- ⁵⁴ Thereza Paiva, Raimundo R. dos Santos, R. T. Scalettar, and P. J. H. Denteneer, “Critical temperature for the two-dimensional attractive Hubbard model,” *Phys. Rev. B* **69**, 184501 (2004).
- ⁵⁵ Xin Zhang, Wei Wu, Gang Li, Lin Wen, Qing Sun, and An-Chun Ji, “Phase diagram of interacting Fermi gas in spin-orbit coupled square lattices,” *New Journal of Physics* **17**, 073036 (2015).
- ⁵⁶ Valentina Brosco and Massimo Capone, “Rashba-metal to Mott-insulator transition,” *Phys. Rev. B* **101**, 235149 (2020).
- ⁵⁷ Welberth Kennedy, Sebastião dos Anjos Sousa-Júnior, Natanael C. Costa, and Raimundo R. dos Santos, “Magnetism and metal-insulator transitions in the Rashba-Hubbard model,” *Phys. Rev. B* **106**, 165121 (2022).
- ⁵⁸ Xuanlan Wang and Wei Zhu, “Intertwined charge and spin orders through the exchange-interaction on a square lattice,” *Physics Letters A* **461**, 128652 (2023).
- ⁵⁹ Masataka Kawano and Chisa Hotta, “Phase diagram of the square-lattice Hubbard model with Rashba-type antisymmetric spin-orbit coupling,” *Phys. Rev. B* **107**, 045123 (2023).
- ⁶⁰ Erik Wegner Hodt, Jabir Ali Ouassou, and Jacob Linder, “Transient dynamics and quantum phase diagram for the square lattice Rashba-Hubbard model at arbitrary hole doping,” *Phys. Rev. B* **107**, 224427 (2023).
- ⁶¹ A. Moreo and D. J. Scalapino, “Two-dimensional negative-U Hubbard model,” *Phys. Rev. Lett.* **66**, 946–948 (1991).
- ⁶² Rodrigo A. Fontenele, Natanael C. Costa, Raimundo R. dos Santos, and Thereza Paiva, “Two-dimensional attractive Hubbard model and the BCS-BEC crossover,” *Phys. Rev. B* **105**, 184502 (2022).
- ⁶³ Ho-Kin Tang, Xiaosen Yang, Jinhua Sun, and Hai-Qing Lin, “Berezinskii-Kosterlitz-Thoules phase transition of spin-orbit coupled Fermi gas in optical lattice,” *Europhysics Letters* **107**, 40003 (2014).
- ⁶⁴ Peter Rosenberg, Hao Shi, and Shiwei Zhang, “Ultra-cold Atoms in a Square Lattice with Spin-Orbit Coupling: Charge Order, Superfluidity, and Topological Signatures,” *Phys. Rev. Lett.* **119**, 265301 (2017).
- ⁶⁵ Andrzej Ptok, Karen Rodríguez, and Konrad Jerzy Kapcia, “Superconducting monolayer deposited on substrate: Effects of the spin-orbit coupling induced by proximity effects,” *Phys. Rev. Mater.* **2**, 024801 (2018).